

1  
2  
3  
4  
5  
6  
7  
8  
9  
10  
11  
12  
13  
14  
15  
16  
17  
18  
19  
20  
21  
22  
23

**Simple Doppler Wind Lidar adaptive observation experiments with 3D-Var  
and an ensemble Kalman filter in a global primitive equations model**

Junjie Liu and Eugenia Kalnay

Dept. of Atmospheric and Oceanic Science, U. of Maryland, College Park, MD 20742

May 16, 2007

## Abstract

1  
2 Through simple Observing System Simulation Experiments, we compare several  
3 adaptive observation strategies designed to subsample Doppler Wind Lidar (DWL)  
4 observations along satellite tracks, and examine the effectiveness of two data assimilation  
5 schemes, 3D-Var and the Local Ensemble Transform Kalman Filter (LETKF). With respect  
6 to sampling strategies, our results show that the LETKF-based ensemble spread method is  
7 superior to the other strategies tested, namely, use of a uniform distribution, the  
8 climatological spread strategy, or use of a random distribution, and is close to the ideal result  
9 obtained assuming that the true forecast error is known. With 10% DWL observations from  
10 the ensemble spread strategy, both 3D-Var and LETKF attain about 90% of the impact that  
11 100% DWL wind profile coverage would provide. However, when the adaptive DWL  
12 observations coverage is reduced to 2%, 3D-Var becomes less effective than the more  
13 advanced LETKF assimilation scheme.

## 11. Introduction

2        Within the next few years, the first Doppler Wind Lidar (DWL) will be deployed in  
3 space by the European Space Agency (ESA, see, <http://www.congrex.nl/06c05/>). In addition,  
4 in its recent Decadal Survey Report, the National Research Council recommended a US  
5 global winds mission in the coming decade. Because the operation of DWL is strongly  
6 constrained by energy resources (Rishojgaard and Atlas, 2004), a frequently stated qualitative  
7 goal is to get about 90% of the total effectiveness from just 10% coverage with adaptive  
8 observations. Here, 10% coverage means making measurements in only 10% of the total  
9 footprints that the DWL can possibly scan in a certain interval such as 6 hours. Unlike the  
10 applications of adaptive dropsonde observing in field experiments (FASTEX, NORPEX,  
11 Joly et al., 1997; Bergot, 1999; Langland et al., 1999a; Langland et al., 1999b; Pu and  
12 Kalnay, 1999; Szunyogh et al., 1999; Majumdar et al., 2002; Toth et al., 2002; Langland  
13 2005), which attempt to optimize the 2-3 days forecast within a specified verification region  
14 (e.g, Europe, or North America), the goal in our study is to optimize the 6-hour global  
15 analysis by optimally distributing the limited DWL observation resources. As pointed out by  
16 Lorenz and Emanuel (1998), if adaptive observations are made at the locations with largest  
17 background uncertainty, the global analysis error will be most reduced as compared to other  
18 locations. The question we address is how to represent the background dynamical uncertainty  
19 and choose adaptive observation locations accordingly.

20        The Ensemble Kalman Filter (EnKF) (Evensen, 1994; Anderson, 2001; Houtekamer and  
21 Mitchell, 2001; Bishop et al., 2001; Whitaker and Hamill, 2002; Ott et al., 2004; Hunt et al.,  
22 2007), a relatively new data assimilation approach, provides an estimate of the background  
23 dynamical uncertainty. We call the diagonal value of an EnKF-computed background error

24 covariance matrix for a given variable the ensemble spread for that variable. Locations with  
25 large ensemble spread are those in which dynamical instabilities of the evolving flow will  
26 result in large background (forecast) error and therefore where observations can be most  
27 useful. The different observation location selection strategies that we compare are (a) one  
28 based on the LETKF ensemble spread, (b) a uniform observation distribution, (c) one based  
29 on the climatological background uncertainty, (d) random locations, and (e) an “ideal”  
30 strategy based on assumed knowledge of the true forecast error. We compare the impacts of  
31 adaptive observations selected with these different methods by assimilating them with two  
32 different data assimilation schemes, 3D-Var and Local Ensemble Transform Kalman Filter  
33 (LETKF). We test both 10% and 2% adaptive observations coverage, allowing for relatively  
34 dense and sparse adaptive observation scenarios. Comparison of these two scenarios will  
35 show the sensitivity of data assimilation schemes to the amount of adaptive observations.

## 36 **2. Model, observations, and data assimilation schemes**

37 In this study, we use the Simplified Parameterizations, primitive Equation Dynamics  
38 (SPEEDY) model, developed by Molteni (2003) and adapted for data assimilation by  
39 Miyoshi (2005). It has a simplified but complete set of physical processes, seven vertical  
40 levels, 96 longitudinal grid points, and 48 latitudinal grid points. We follow a “perfect model”  
41 Observing System Simulation Experiments (OSSEs) setup, in which the simulated “truth”  
42 (long model integration) is generated with the same atmospheric model as the one used in  
43 data assimilation. In such an experimental setup, we avoid the complications of model error,  
44 and the only source of forecast errors comes from the initial conditions. Observations are  
45 obtained from the “truth” with added Gaussian random perturbations. The observation error

46 standard deviations assumed for wind components ( $u$ ,  $v$ ), temperature ( $T$ ), specific humidity  
47 ( $q$ ) and surface pressure ( $p_s$ ) are 1.0m/s, 1.0K, 0.1g/kg, and 1.0hPa, respectively.

48 To test the sensitivity of the impacts of adaptive observations to data assimilation  
49 methods, we use both 3D-Var (Parrish and Derber, 1998, Miyoshi, 2005) and LETKF (Ott et  
50 al., 2004; Hunt et al., 2007). 3D-Var uses a constant background error covariance, which is  
51 calculated as in Parrish and Derber (1998). LETKF, a newly developed scheme belonging to  
52 EnKF family, employs the time evolving error covariance estimated from the forecast  
53 ensemble. It automatically gives the estimation of the forecast uncertainty. The application of  
54 LETKF on the SPEEDY model follows Hunt et al. (2007).

### 55 **3. Adaptive strategies and the distribution of simulated adaptive DWL observations**

56 We mimic satellite tracks and DWL observations assuming that the satellite scans half  
57 hemisphere “orbits” in each 6- hour analysis cycle. The basic observations ( $u$ ,  $v$ ,  $T$ ,  $q$ ,  $p_s$ )  
58 assimilated in all our experiments are simulated rawinsondes, shown as closed circles in  
59 Figure 1 (6 hr “orbits” are shown separated by vertical dashed lines). Figure 1 also shows an  
60 example of the distribution of 10% adaptive observations (crosses) from the ensemble spread  
61 strategy (defined below) at 1200 UTC. At 0000 UTC, the satellite scans the same half  
62 hemisphere orbit as at 1200 UTC, and the other half hemisphere orbit is scanned at 0600  
63 UTC and 1800 UTC. Thus, we assume that each grid point can be observed twice a day (this  
64 is too optimistic because we neglect the impact of clouds). Since the characteristics of the  
65 forecast uncertainties are different in different regions (Kalnay, 2003), the adaptive DWL  
66 observations are distributed into seven subregions, the equatorial region, the northern and  
67 southern tropics, and northern and southern mid- and high-latitudes (separated by horizontal  
68 dashed lines in Fig. 1). Each subregion is allotted a number of adaptive observations

69 proportional to its area. At the selected adaptive DWL locations, both zonal wind and  
70 meridional wind are observed at all vertical levels, which is also over-optimistic because the  
71 lidar wind component that is actually observed is its projection on the line-of-sight direction  
72 (Stoffelen et al., 2005).

73         In all of the five adaptive observation strategies we tested, we impose a horizontal  
74 separation constraint to minimize possible observation redundancy, namely that the adaptive  
75 observations have to be at least two grid points apart in both longitude and latitude directions.  
76 Hamill and Snyder (2002) account for observation redundancy by selecting the observations  
77 serially in minimizing the analysis error variance. However, directly minimizing the analysis  
78 error variance is much more expensive than computing ensemble spread and applying the  
79 separation constraint, especially when selecting adaptive observations from a very large pool  
80 of observation locations. Moreover, by selecting adaptive observations at the locations with  
81 large ensemble spread in ensemble spread strategy, we indirectly minimize the analysis error  
82 variance. The separation constraint is done by first ordering the average 6-hour forecast  
83 ensemble spread of wind at 500hPa from largest to smallest in each region. Within each  
84 region, the location with largest ensemble spread is selected as the first adaptive observation  
85 location. Then, we delete the locations adjacent to the first adaptive observation location in  
86 both zonal and meridional direction from the potential adaptive observation queue. The  
87 second adaptive observation location is where ensemble spread in the remaining queue is  
88 largest. This process is repeated until all the adaptive observation locations are selected. If all  
89 the observations are either selected or deleted before the allotted number of adaptive  
90 observations are picked out, the remaining adaptive observations are the locations with  
91 largest ensemble spread that were deleted from the queue. A similar separation constraint is

92 applied in all of the other strategies. In the climatological spread method, the climatological  
93 background ensemble spread is obtained from LETKF analyses of rawinsondes observations,  
94 and the adaptive observations are at the locations with largest climatological ensemble  
95 spread. In the ideal strategy, the adaptive observations are located where the background error  
96 (i.e., the absolute difference between 6-hour forecasts of 500hPa wind and the true 500hPa  
97 wind field) is largest. Since this strategy requires knowing the “truth”, it cannot be  
98 implemented in practice. The adaptive observation locations from ensemble spread, random  
99 location and the ideal strategy change with time, whereas the locations are fixed for uniform  
100 distribution and climatological ensemble spread strategies. In order to test whether the  
101 forecast ensemble spread truly represents forecast uncertainty, we use the same adaptive  
102 observation locations for both 3D-Var and LETKF in the ensemble spread and climatological  
103 ensemble spread strategies, even though they are both derived from LETKF assimilations.

104 We examine the effectiveness of these five adaptive observation strategies by  
105 computing the analysis Root Mean Square (RMS) errors and comparing them to extremes of  
106 both 0% DWL coverage (i.e., rawinsondes only), and full (100%) DWL coverage. The

107 percentage improvement for each strategy is defined as  $PI = \frac{RMS - RMS^{0\%}}{RMS^{100\%} - RMS^{0\%}} \times 100\%$ ,

108 where  $RMS$  is the time mean global average RMS error of the adaptive strategy,  
109  $RMS^{100\%}$  and  $RMS^{0\%}$  are the time mean global average RMS error of full DWL coverage and  
110 no DWL coverage, respectively.

#### 111 **4. Results**

112 Figure 2 shows the time evolution of the global averaged zonal wind analysis RMS  
113 errors for 3D-Var (left) and LETKF (right) with 0% coverage (solid line with crosses) and  
114 100% coverage (solid line), as well as the five adaptive strategies using 10% coverage. The

115 time averaged RMS error for the second month is presented in Table 1. Not surprisingly, the  
116 ideal strategy (dot dashed line) has the smallest errors, and is close to the 100% coverage. The  
117 LETKF-based ensemble spread strategy (solid line with open squares) is the best of the  
118 adaptive strategies that are feasible in practice, and is very close to the ideal strategy even for  
119 the 3D-Var analysis. The random location (dashed line) is better than the uniform distribution  
120 strategy (solid line with closed circles). The worst results are obtained from the climatological  
121 ensemble spread distribution (solid line with open circles) because there are no adaptive  
122 observations over vast areas (not shown). The adaptive strategies with time-changing  
123 locations (ensemble spread, random location, ideal strategy) are all better than the constant  
124 observation distributions (uniform distribution, climatological ensemble spread), a conclusion  
125 consistent with previous results (Lorenz and Emanuel, 1998; Hamill and Snyder, 2002).  
126 Through the covariance between winds and the other variables in background error  
127 covariance, the wind observations improve the analysis of the other variables as well, such as  
128 temperature (not shown). The different adaptive observation strategies have the same ranking  
129 as for the wind analysis.

130       A striking result is that the RMS error of LETKF (Fig. 2b and Table 1) shows a much  
131 smaller difference among the adaptive strategies than that of 3D-Var, although their relative  
132 ranking is the same. This is because 3D-Var, with a constant background error covariance, is  
133 much more sensitive to the choice of observations. With less optimal adaptive strategies, such  
134 as uniform distribution, the large background errors are not effectively reduced due to lack of  
135 observations around some locations with large background error (left panel in Fig. 3). On the  
136 other hand, with the ensemble spread strategy, the adaptive observations are near the  
137 locations with large background errors (right panel in Fig. 3). Therefore, the assimilation of

138 these adaptive observations is equivalent to providing the information of the time-changing  
139 large background errors to 3D-Var. As a result, the analysis increments in 3D-Var have a  
140 shape more similar (but with opposite sign) to the background error (Fig. 3, right) than in any  
141 other feasible method. By contrast, LETKF, whose background error covariance already  
142 includes information on the “errors of the day”, is more efficient in extracting information  
143 from the observations even if their locations are not optimal, so that all the strategies give  
144 similarly small analysis errors.

145       It is clear from Figure 2a and Table 1 that 3D-Var attains more than 90% of the  
146 improvements between 0% and 100% coverage from just 10% adaptive observations  
147 determined with the ensemble spread strategy. The percentage improvement of ensemble  
148 spread strategy in LETKF is somewhat smaller than for 3D-Var, and, as discussed above, all  
149 adaptive strategies are similarly successful (Table 1). This seems to contradict to the  
150 conclusions based on the previous adaptive observation field experiments that adaptive  
151 observations would be more effective with more advanced data assimilation schemes, such as  
152 4D-Var or EnKF (Langland, 2005). However, we used relatively dense adaptive observation  
153 coverage in our experiments with 10% observed every 6 hours over half the globe. To make  
154 our results more compatible with previous field experiments, we now use the same adaptive  
155 observation strategies but substantially reduce the number of observation locations to only  
156 2% of the full coverage (Table 2). With this small number of adaptive observations, the  
157 analysis errors of the adaptive strategies in 3D-Var are much larger, and even the most  
158 effective strategies, random location and ensemble spread, are only able to reduce the errors  
159 by less than 30%. By contrast, the LETKF still obtains 77% improvements from just 2%  
160 adaptive observations. The difference in performance among the five adaptive observation

161 strategies is much more evident, but with the same ranking as before. This result shows that  
162 with fewer adaptive observations, the data assimilation scheme plays a more important role in  
163 determining the effectiveness of adaptive observations. More advanced data assimilation  
164 schemes, such as the LETKF, use more efficiently of small amounts of observation  
165 information, which is consistent with previous field experiments (Langland, 2005). The small  
166 number of observations is not enough to provide enough global information on the “errors of  
167 the day” needed for the improvement of 3D-Var, while in the LETKF, it is possible to  
168 estimate the evolving error structures even with few observations.

## 169 **5. Conclusions and discussion**

170 In this study we showed the potential of a simple ensemble spread strategy for adaptive  
171 observations in the context of minimizing the energy required by DWL laser firings. The  
172 same adaptive strategy could be used for any satellite instrument designed to “dwell” in  
173 regions of high uncertainty rather than providing uniform coverage along the orbit as  
174 conventionally done.

175 We compared ensemble spread with several other adaptive observation strategies  
176 (uniform distribution, random distribution, climatological ensemble spread) and found that  
177 the 6-hour LETKF forecast ensemble spread gives a useful estimate of background  
178 uncertainty and dynamical instabilities. With 10% adaptive DWL observations, the ensemble  
179 spread sampling strategy gives the best result in both 3D-Var and LETKF, attaining more  
180 than 90% effectiveness of the full observation coverage. 3D-Var is more sensitive to adaptive  
181 strategies than the LETKF. Since the latter includes information on the “errors of the day”,  
182 different adaptive strategies have closer performances.

183 We found that the sensitivity of adaptive observation effectiveness to data assimilation  
184 schemes is related to the amount of adaptive observations to be determined. With a relatively  
185 dense number of adaptive wind observations, such as 10% of the maximum coverage, 3D-Var  
186 can be as effective as LETKF, a more advanced data assimilation schemes. With only 2%  
187 coverage, 3D-Var is not as effective as LETKF even when using the LETKF ensemble spread  
188 locations.

189 Although our results are indicative of the potential for adaptive observations in remote  
190 sensing, we made several simplifying assumptions, using a perfect model scenario, a low  
191 resolution global model, an extreme simplification of satellite orbits and DWL observations,  
192 assuming uncorrelated Gaussian observation errors, and neglecting the effect of clouds. As a  
193 result, the actual percentage improvements from assimilating DWL adaptive observations  
194 may be overoptimistic. Experiments with state-of-the-art OSSE systems should be carried out  
195 to verify whether our results are valid in a more realistic setup. We believe that the main  
196 results (that the EnKF-based uncertainty estimation gives valuable guidance to allocate  
197 limited observation resources along the satellite track, and that the effectiveness of data  
198 assimilation schemes is sensitive to the amount of adaptive observations) would be valid even  
199 in a realistic experimental setup.

## **Acknowledgements**

We are very grateful to Drs. Wayman Baker, David Emmitt and Bob Atlas for their encouragement and suggestions, and to our colleagues from the Weather and Chaos group at the University of Maryland, especially Profs. Ed Ott, Istvan Szunyogh, and Brian Hunt, for many discussions. This work was supported by a NOAA/NASA/NPOESS grant through SWA04N0024403C.

## **References**

- Anderson, J. L. (2001), An ensemble adjustment Kalman filter for data assimilation. *Mon. Weather Rev.*, 129, 2884-2903.
- Bergot, T. (1999), Adaptive observations during FASTEX: a systematic survey of upstream flights. *Quart. J. Roy. Meteor. Soc.* 125, 3271-3298
- Bishop, C. H., B. Etherton, and S. J. Majumdar (2001), Adaptive sampling with the ensemble transform Kalman filter. Part : Theoretical aspects. *Mon. Weather Rev.*, 129, 420-436
- Evensen, G. (1994), Sequential data assimilation with a nonlinear quasi-geostrophic model using Monte Carlo methods to forecast error statistics. *J. Geophys. Res.*, 99 (C5), 10 143-10 162.
- Hamill, M. T. and C. Snyder (2002), Using improved background-error covariances from an ensemble Kalman filter for adaptive observations. *Mon. Weather Rev.*, 130, 1552-1572.
- Houtekamer, P. L., and H. L. Mitchell (2001), A sequential Ensemble Kalman Filter for atmospheric data assimilation. *Mon. Weather Rev.*, 129, 123-137.
- Hunt, B. R., E. J., Kostelich, and I., Szunyogh (2007), Efficient Data Assimilation for Spatiotemporal Chaos: a Local Ensemble Transform Kalman Filter. *Physics D.* (in press)
- Joly, A., and Coauthors (1997), Definition of the Frants and Atlantic Storm-Track Experiment (FASTEX). *Bull. Amer. Meteor. Soc.*, 78, 1917-1940.

- Kalnay, E. (2003), *Atmospheric modeling, data assimilation and predictability*, 341pp, Cambridge Univ. Press, New York.
- Langland, R. H., R., Gelaro, G. D., Rohaly and M. A., Shapiro (1999a), Targeted observations in FASTEX: Adjoint-based targeting procedures and data impact experiments in IOP17 and IOP18. *Quart. J. Roy. Meteor. Soc.*, *125*, 3241-3270.
- Langland, R. H., and Coauthors (1999b), The North Pacific Experiment (NORPEX-98): Targeted Observations for Improved North American Weather Forecasts. *Bull. Amer. Meteor. Soc.*, *80*, 1363-1384
- Langland, R. H. (2005), Issues in targeted observing. *Q. J. R. Meteor. Soc.*, *131*, 3409-3425.
- Lorenz, E. N. and K. A. Emanuel (1998), Optimal sites for supplementary observations: Simulation with a small model. *J. Atmos. Sci.*, *55*, 399-414.
- Majumdar, S. J., C. H. Bishop, and B. J. Etherton (2002), Adaptive sampling with the ensemble transform Kalman filter. Part II: Field program implementation. *Mon. Weather Rev.*, *130*, 1356-1369.
- Miyoshi, T. (2005), Ensemble Kalman filter experiments with a primitive-equation global model, Ph. D thesis, University of Maryland.
- Molteni, F. (2003), Atmospheric simulations using a GCM with simplified physical parametrizations. I: Model climatology and variability in multi-decadal experiments. *Climate Dyn.*, *20*, 175-191.
- Ott, E., B. R. Hunt, I. Szunyogh, A. V. Zimin, E. J. Kostelich, M. Corazza, E. Kalnay, D. J. Patil, and J. A. Yorke, (2004), A Local Ensemble Kalman Filter for Atmospheric Data Assimilation. *Tellus*, *56A*, 415-428

- Parrish, D. F., and J. C. Derber (1992), The National Meteorological Center's spectral statistical-interpolation analysis system. *Mon. Weather Rev.*, 120, 1747-1763
- Pu, Z., and E. Kalnay (1999), Targeting observations with the quasi-inverse linear and adjoint NCEP global models: Performance during FASTEX. *Q. J. R. Meteor. Soc.*, 125, 3329-3338
- Rishojgaard, L. P., R. Atlas (2004), The impact of Doppler Lidar Wind observations on a Single-Level meteorological analysis. *J. of Applied Meteorology*, 43, 810-820.
- Stoffelen, A. and Coauthors (2005), The atmospheric dynamics mission for global wind field experiments. *Bull. Amer. Meteor. Soc.*, 86, 73-87
- Szunyogh, I., Z., Toth, K. A. Emanuel, C. H. Bishop, C. Snyder, R. E. Morss, J. S. Woolen, and T. P. Marchok (1999), Ensemble-based targeting during FASTEX: the impact of dropsonde data from the LEAR jet. *Quart. J. Roy. Meteor. Soc.*, 125, 3189-3217.
- Toth, Z. and Coauthors (2002), Adaptive observations at NCEP: Past, present and future. Preprints of the Symposium on Observations, Data assimilation and Probabilistic Prediction, *Orlando FL, 13-17 January 2002, 185-190.*
- Whitaker, J. S., and T. M. Hamill (2002), Ensemble data assimilation without perturbed observations. *Mon. Weather Rev.* 130, 191

## List of figures

Fig. 1 Example of the distribution of adaptive observations (crosses) from the ensemble spread sampling strategy at 1200 UTC February 03. The closed circles represent rawinsonde observation locations. Shades represent the average ensemble spread of zonal and meridional wind at 500hPa at that time. Horizontal dashed lines divide the whole globe into seven latitude bands. Vertical dashed lines separate the globe into four sub-regions representing two “orbits”.

Fig. 2 2-month evolution of 500hPa globally averaged zonal wind analysis RMS errors for 3D-Var (left panel) and LETKF (right panel) from 10% adaptive observations assimilation. From top to bottom their order is solid line with crosses: rawinsonde observation (0% DWL) assimilation; solid line with open circles: climatological spread; solid line with closed circles: uniform distribution; dashed line: random locations; solid line with open squares: ensemble spread adaptive strategy; dot dashed line: ideal sampling; solid line without marks: 100% adaptive observation coverage over half hemisphere.

Fig. 3 3D-Var zonal wind analysis increments (contour interval 0.3m/s), background error (shaded) and adaptive observation distribution (crosses) from uniform distribution (left panel) and from ensemble spread sampling strategy (right panel) at 1200 UTC February 03. The closed circles are rawinsonde observation locations.

Table 1 500hPa zonal wind time average (over February) of global mean RMS errors and percentage improvement (PI) of 10% adaptive observations for both 3D-Var and LETKF.

Data assimilation	Experiment	Rawinsonde (0%)	Climatology (10%)	Uniform (10%)	Random (10%)	Spread (10%)	Ideal (10%)	100%
3D-Var	RMS error (m/s)	4.04	2.36	0.92	0.74	0.43	0.36	0.30
	PI	N/A	45%	83%	88%	97%	98%	N/A
LETKF	RMS error (m/s)	1.18	0.38	0.36	0.33	0.32	0.29	0.23
	PI	N/A	84%	84%	89%	91%	94%	N/A

Table 2 500hPa zonal wind time average (over February) of global mean RMS errors and percentage improvement (PI) of 2% adaptive observations for both 3D-Var and LETKF.

Data assimilation	Experiment	Rawinsonde (0%)	Climatology (2%)	Uniform (2%)	Random (2%)	Spread (2%)	Ideal (2%)	100%
3D-Var	RMS error (m/s)	4.04	3.26	3.53	3.00	3.11	1.68	0.30
	PI	N/A	21%	14%	28%	25%	63%	N/A
LETKF	RMS error (m/s)	1.18	0.67	0.59	0.51	0.45	0.41	0.23
	PI	N/A	54%	62%	71%	77%	81%	N/A

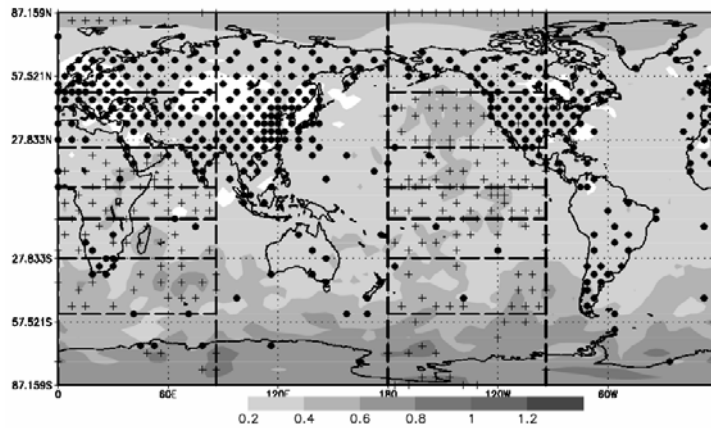


Fig. 1 Example of the distribution of adaptive observations (crosses) from the ensemble spread sampling strategy at 1200 UTC February 03. The closed circles represent rawinsonde observation locations. Shades represent the average ensemble spread of zonal and meridional wind at 500hPa at that time. Horizontal dashed lines divide the whole globe into seven latitude bands. Vertical dashed lines separate the globe into four sub-regions representing two "orbits".

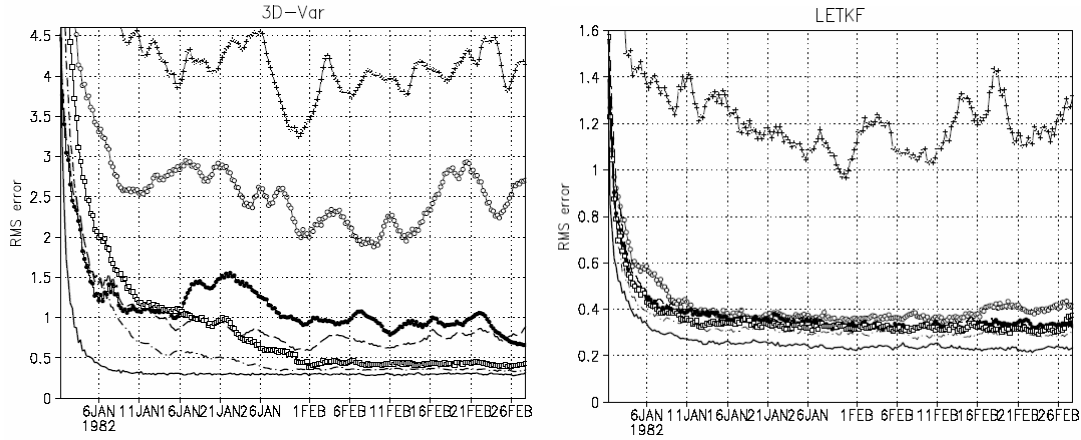


Fig. 2 2-month evolution of 500hPa globally averaged zonal wind analysis RMS errors for 3D-Var (left panel) and LETKF (right panel) from 10% adaptive observations assimilation. From top to bottom their order is solid line with crosses: rawinsonde observation (0% DWL) assimilation; solid line with open circles: climatological spread; solid line with closed circles: uniform distribution; dashed line: random locations; solid line with open squares: ensemble spread adaptive strategy; dot dashed line: ideal sampling; solid line without marks: 100% adaptive observation coverage over half hemisphere.

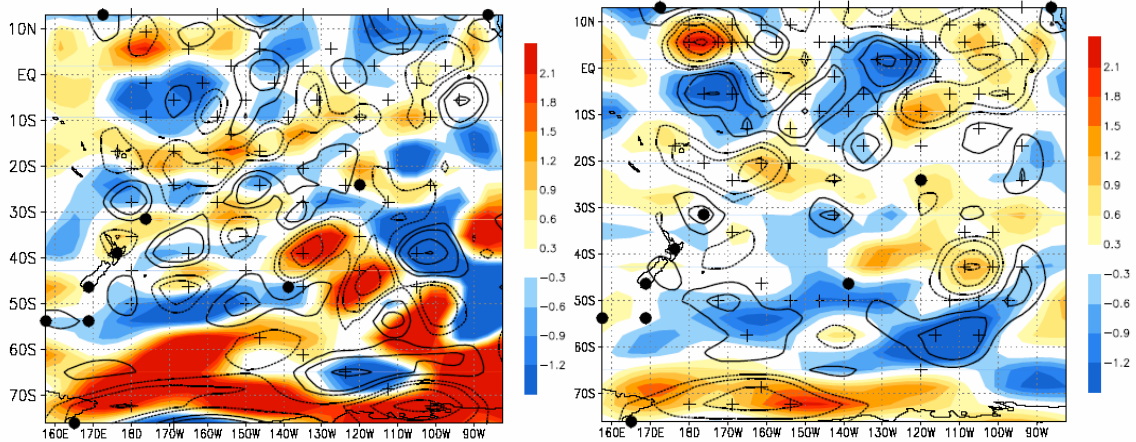


Fig. 3 3D-Var zonal wind analysis increments (contour interval 0.3m/s), background error (shaded) and adaptive observation distribution (crosses) from uniform distribution (left panel) and from the ensemble spread sampling strategy (right panel) at 1200 UTC February 03. The closed circles are rawinsonde observation locations.